

Non-unitary Variational Quantum Eigensolver with the Localized Active Space Method and Cost Mitigation

Qiaohong Wang,[†] Ruhee D’Cunha,[‡] Abhishek Mitra,[‡] Yuri Alexeev,[¶] Stephen K.
Gray,^{*,§} Matthew Otten,^{*,||} and Laura Gagliardi^{*,‡}

[†]*Pritzker School of Molecular Engineering, University of Chicago, Chicago, IL 60637, USA.*

[‡]*Department of Chemistry, Chicago Center for Theoretical Chemistry, University of
Chicago, Chicago, IL 60637, USA.*

[¶]*NVIDIA Corporation, 2788 San Tomas Express Way, Santa Clara, CA 95051*

[§]*Center for Nanoscale Materials, Argonne National Laboratory, 9700 S. Cass Avenue,
Lemont, IL 60439*

^{||}*Department of Physics, University of Wisconsin – Madison, Madison, WI 53726, USA*

E-mail: gray@anl.gov; mjotten@wisc.edu; lgagliardi@uchicago.edu

Abstract

Accurately describing strongly correlated systems with affordable quantum resources remains a central challenge for quantum chemistry applications on near and intermediate term quantum computers. The localized active space self-consistent field (LASSCF) approximates the complete active space self-consistent field (CASSCF) by generating active space-based wave functions within specific fragments while treating interfragment correlation with mean-field approach, hence is computationally less expensive. Hardware-efficient ansatzes (HEA) offer affordable and shallower circuits,

yet they often fail to capture the necessary correlation. Previously, Jastrow-factor-inspired non-unitary qubit operators were proposed to use with HEA for variational quantum eigensolver (VQE) calculations (so-called nuVQE), as they do not increase circuit depths and recover correlation beyond the mean-field level for Hartree-Fock initial states. Here, we explore running nuVQE with LASSCF as the initial state. The method, named LAS-nuVQE, is shown to recover interfragment correlations, reach chemical accuracy with a small number of gates (<70) in both H_4 and square cyclobutadiene (C_4H_4), and produces more accurate energetics than its HEA counterparts at all circuit depths. To further address the inherent symmetry-breaking in HEA, we implemented spin-constrained LAS-nuVQE to extend the capabilities of HEA further and show spin-pure results for square cyclobutadiene. We also mitigate the increased measurement overhead of nuVQE via Pauli grouping and shot-frugal sampling, reducing measurement costs by up to two orders of magnitude compared to ungrouped operator, and show that one can achieve better accuracy with a small number of shots (10^{3-4}) per one expectation value calculation compared to noiseless simulations with one or two orders of magnitude more shots. Finally, wall clock time estimates show that, with our measurement mitigation protocols, nuVQE becomes a cheaper and more accurate alternative than vanilla VQE with HEA. Taken together, these developments illustrate a practical pathway toward performing multireference chemical simulations with accuracy and affordable resources on today’s quantum hardware, achieving both accuracy and affordability in challenging correlated systems.

I. Introduction

In recent decades, advances in quantum computing have led to new approaches to simulate many-body quantum systems; these show great promise owing to their polynomial scaling of quantum resources needed to solve otherwise exponentially complex quantum mechanical problems.¹⁻⁴ In the noisy, intermediate-scale quantum (NISQ) era,⁵ hybrid algorithms such as the variational quantum eigensolver (VQE) are the most researched and developed choices

for ground-state energy calculations of molecules.^{6–9} VQE approximates the lowest eigenvalue (i.e. ground-state) of a given operator (i.e. Hamiltonian) through the Rayleigh-Ritz variational principle. The algorithm iteratively adjusts parameters in a trial quantum circuit (a so-called ansatz) to minimize the expectation value of the Hamiltonian, which is calculated through measurements after each circuit’s execution. The quantum state prepared with the optimal parameters hence represents the molecule’s ground-state electronic wave function. As a result, the desired physical state is limited by the capability of the trial state and the affordability of the circuit depth. The search for an accurate and easy-to-prepare variational ansatz is an ongoing area of research. The variety of established variational ansatzes for VQE on quantum devices can be categorized into two families: 1) hardware-efficient ansatzes (HEA) and 2) the chemically inspired unitary coupled cluster (UCC) ansatz, which was proposed to be used with VQE.⁷ Classically, UCC generates a non-terminating Baker-Campbell-Hausdorff series with a fixed excitation rank,¹⁰ making it exponentially scaling for classical computers but only of polynomial complexity with Trotterization on a quantum computer.¹¹ However, a large prefactor of the UCC and its expensive circuit depths (scales as $O(N_q^4)$ with the N_q number of qubits) limit its feasibility in NISQ devices, motivating the HEA as an alternative.^{6,12} The HEA (or heuristic ansatz) is designed to be efficiently implemented with gates natively available on quantum devices and is thus computationally advantageous. It usually leads to shallow circuit depths, which are necessary with hardware limitations such as coherence time. However, a potential flaw lies in the non-chemically motivated nature of the construction of HEA, as it does not guarantee the conservation of physical properties, such as spin and the number of particles.¹³

Much progress has been made to reduce the complexity of UCC and develop alternative methods to provide an accurate and compact wave function ansatz. Several variations and derivatives of UCC include the qubit coupled-cluster ansatz,¹⁴ unitary paired CC ansatz,¹⁵ iterative ansatzes like ADAPT-VQE and qubit ADAPT-VQE,^{16,17} selective schemes like the unitary selective coupled-cluster (USCC) ansatz.^{18,19} Another direction draws inspira-

tion from the classical quantum Monte Carlo method, namely the unitary cluster Jastrow ansatz.²⁰ Efforts towards this direction include the local unitary cluster Jastrow ansatz,²¹ Jastrow quantum circuit,²² and non-unitary VQE with linearized qubit Jastrow operators,²³ which we explore in this work.

A qualitatively good initial state is another key to the VQE algorithm. Multireference theory is indispensable to tackle complex electronic structure calculations, such as bond breaking, excited states, radicals, and transition-metal complexes.²⁴ Localized active space self-consistent field (LASSCF),^{25,26} also known as the cluster mean-field (cMF) method,²⁷ approximates the paradigmatic multireference theory complete active space self-consistent field (CASSCF)²⁸ by further partitioning the active space into fragments, ideally reducing the computational cost to linear with respect to the number of such fragments. The underlying assumption is that the electrons are strongly correlated in an active space that can be further separated into weakly interacting regions, resulting in a wave function in the form of an antisymmetrized product of fragment wave functions. LASSCF has been shown to predict spin-state energy gaps similar to those of CASSCF for bimetallic compounds,²⁹ describe accurate dissociations of two double bonds in bisdiazene,²⁶ and produce a more consistent orbital evolution throughout the potential energy surface of sulfonium salts compared to CASSCF.³⁰ However, when electron correlation between fragments becomes important, the LASSCF approximation is too drastic, leading to inaccuracies. Restoring lost correlations classically using the variational,³¹ perturbative,^{32,33} or CC approach³⁴ is challenging for it usually requires building a many-body basis for each fragment. As a consequence, these approaches carry over the complexities inherent in multireference perturbation and CC theories.

The localized active space unitary coupled cluster (LAS-UCC) method successfully reintroduces correlations between LASSCF fragments with the aforementioned variational UCC ansatz with single and double excitations in a VQE scheme,³⁵ which allows accurate studies of multireference systems on quantum computers. However, with hardware limitations in the

NISQ era, running a LAS-UCC hardware calculation for relevant systems is impractical on current hardware. To reduce the cost, localized active space unitary selective coupled cluster (LAS-USCC)¹⁹ has been introduced, yet it might still be unrealistic to run while producing accurate results on near-term devices. Recently, Benfenati et al. formulated non-unitary VQE (nuVQE) method with HEA²³ and showed that it produces more accurate energies for small molecules compared to just VQE with the same HEA at the same circuit depths. This approach could in principle provide another direction to recover interfragment correlations lost from LASSCF and study multireference systems with accuracy on quantum hardware with much more affordable NISQ quantum resources.

In this paper, we use LASSCF as the initial state to carry out nuVQE calculations with HEA. LASSCF provides a qualitatively good wave function as a starting point, and nuVQE ensures the affordability of quantum resources and improved accuracy compared to vanilla VQE with HEA. The rest of the paper is laid out as follows: In Section II., we introduce the theory and formulations of LASSCF, nuVQE, and LAS-nuVQE. In Section III., we benchmark LAS-nuVQE performance on H_4 and square cyclobutadiene. We also present a spin-constrained implementation of LAS-nuVQE. In addition, we showcase strategies to mitigate the measurement costs of nuVQE. Lastly, we provide resource estimation of wall clock time for one query, showing the scalability of our methods. In Section IV, we provide some conclusions and discuss future directions.

II. Theoretical background and computational methods

LASSCF

Multireference methods like CASSCF and multireference configuration interaction (MRCI)^{36,37} scale combinatorially with the number of electrons and orbitals, therefore presenting bottlenecks for large active spaces. Efforts to reduce the cost of CASSCF on classical computers include generalized active space (GAS),³⁸⁻⁴¹ restricted active space (RAS),^{42,43} density-matrix

renormalization group (DMRG)⁴⁴⁻⁴⁸ self-consistent field^{49,50} and LASSCF.^{25,26}

The LASSCF energy is optimized by variationally minimizing

$$E_{LAS} = \langle LAS | \hat{H} | LAS \rangle \quad (1)$$

where \hat{H} is the molecular Hamiltonian. The wave function ansatz is

$$|LAS\rangle = \bigwedge_K (\Psi_{A_K}) \wedge \Phi_D \quad (2)$$

where Ψ_{A_K} is a general many-body wave function to describe electrons occupying active orbitals of the K -th fragment, and Φ_D is a single determinant spanning the complement of the complete active space. The wedge operator \bigwedge means that the active space wave function is an anti-symmetrized product of the fragment wave functions Ψ_{A_K} .

Classically solving LASSCF results in a fragmented orbital space and an effective Hamiltonian that is the sum of the local fragment Hamiltonians. Then, the fragment Hamiltonian goes through a fermion-to-spin transformation like the Jordan-Wigner transformation⁵¹ to result in a qubit Hamiltonian, which is to prepare the fragment wave function with QPE circuits, direct initialization (DI), or VQE.⁵² We denote with

$$|\Psi_{QLAS}\rangle = \bigwedge_K (\Psi_{A_k}) \quad (3)$$

the active-space LASSCF wave function loaded onto a quantum device. The wedge operator \bigwedge has the same meaning as the one in eq (2).

Non-unitary VQE

To fully capitalize on the short-circuit depths of HEA, nuVQE is one approach that increases the accuracy of the HEA without adding more gate operators to the circuit, ensuring the practicality of the algorithm in NISQ limitation. Generally, a nonunitary operator $\hat{O}(\vec{\lambda})$ and

a unitary operator $\hat{U}(\vec{\theta})$ can be applied to an initial state $|\Psi_0\rangle$. The wave function can be expressed as

$$|\Psi^o(\vec{\theta})\rangle = \hat{O}(\vec{\lambda})\hat{U}(\vec{\theta})|\Psi_0\rangle = \hat{O}(\vec{\lambda})|\Psi(\vec{\theta})\rangle, \quad (4)$$

where $\hat{U}(\vec{\theta})|\Psi_0\rangle$ is the HEA that evolves the initial states with some unitary gates, resulting in the trial wave function $|\Psi(\vec{\theta})\rangle$. After applying operator $\hat{O}(\vec{\lambda})$, the energy of the wave function is given by

$$E = \frac{\langle \Psi^o(\vec{\theta}) | \hat{H} | \Psi^o(\vec{\theta}) \rangle}{\langle \Psi^o(\vec{\theta}) | \Psi^o(\vec{\theta}) \rangle}, \quad (5)$$

which can be re-expressed as

$$E = \frac{\langle \Psi(\vec{\theta}) | \hat{O}^\dagger(\vec{\lambda}) \hat{H} \hat{O}(\vec{\lambda}) | \Psi(\vec{\theta}) \rangle}{\langle \Psi(\vec{\theta}) | \hat{O}^\dagger(\vec{\lambda}) \hat{O}(\vec{\lambda}) | \Psi(\vec{\theta}) \rangle}. \quad (6)$$

Noticeably, implementing non-unitary operations as eq (5) is challenging. One can implement it on a gate-based quantum computer by adding ancillary qubits, as described in.⁵³ Eq (6), on the other hand, keeps the shallow HEA circuit and allows one to calculate the expectation values of $\hat{O}^\dagger \hat{H} \hat{O}$ and $\hat{O}^\dagger \hat{O}$ while optimizing parameters $\vec{\lambda}$ and $\vec{\theta}$. This formulation can introduce chemically-inspired non-unitary operators while maintaining the same circuit depth as a vanilla VQE with HEA, with the only extra price of the additional measurement of the wave function, which is not normalized.

Many potential forms of non-unitary operators exist and the Jastrow factors⁵⁴ used in Quantum Monte Carlo methods⁵⁵ are classically formulated to introduce accurate and explicitly correlated wave functions beyond the mean-field level. Recent work in the field has constructed qubit operators inspired by one-body and two-body Jastrow factors²³ in the form of

$$J = J_1 + J_2 \quad (7)$$

where

$$J_1 = \exp \left[- \sum_{i=1}^N \alpha_i Z_i \right], J_2 = \exp \left[- \sum_{i<j=1}^N \lambda_{i,j} Z_i Z_j \right], \quad (8)$$

where α_i and $\lambda_{i,j}$ are real coefficients that are sampled from a uniform distribution, and $Z_i = \otimes_j (I_2)_{j \neq i} (Z)_{j=i}$, where i, j are qubit indices. In addition, the authors approximate the operator by linearizing it to further reduce the terms needed for the measurement in the form of

$$J(\vec{\alpha}, \vec{\lambda}) = 1 - \sum_{i=1}^N \alpha_i Z_i - \sum_{i<j=1}^N \lambda_{i,j} Z_i Z_j, \quad (9)$$

LAS-nuVQE

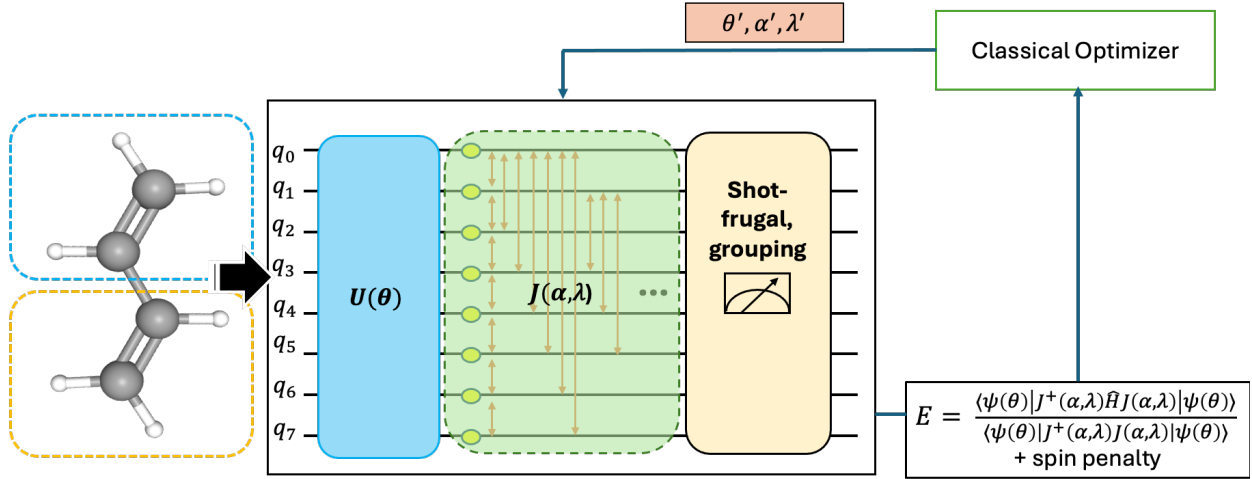


Figure 1: Flowchart describing the LAS-nuVQE algorithm. *Left to right*: An example molecular system solved with LASSCF, where two boxes indicate fragmentation. We then prepare a parameterized HEA with LASSCF as the initial state with the DI method. One-body and two-body Jastrow parameters are classically generated, the dashed lines indicate that the Jastrow parameters do not operate on the circuit. The yellow measurement block illustrates the grouping and shot-frugal techniques one can implement to mitigate measurement costs for the energy evaluation. Lastly, the classical optimizer gives the next set of parameters to optimize the energy expression until convergence variationally.

The LAS-nuVQE algorithm is illustrated in Fig.1 and explained step-by-step in Algorithm 1. The extra number of classical parameters introduced by the Jastrow operators scales as

Algorithm 1 Localized active space non-unitary variational quantum eigensolver

- 1: Prepare the LASSCF wave function on the quantum computer with DI, construct hardware-efficient ansatz
 - 2: Generate a set of parameters defining J_1 and J_2 , and calculate Pauli strings for $\hat{J}^\dagger \hat{H} \hat{J}$ and $\hat{J}^\dagger \hat{J}$.
 - 3: Minimize the energy expression in eq (10) by variationally optimizing the $\vec{\theta}, \vec{\alpha}, \vec{\lambda}$ parameters using a classical optimizer.
-

$\frac{1}{2}N_q(N_q + 1)$, where N_q is the number of qubits. The cost function is defined as

$$E = \frac{\langle \Psi_{QLAS}(\vec{\theta}) | \hat{J}^\dagger(\vec{\alpha}, \vec{\lambda}) \hat{H}_{QLAS} \hat{J}(\vec{\alpha}, \vec{\lambda}) | \Psi_{QLAS}(\vec{\theta}) \rangle}{\langle \Psi_{QLAS}(\vec{\theta}) | \hat{J}^\dagger(\vec{\alpha}, \vec{\lambda}) \hat{J}(\vec{\alpha}, \vec{\lambda}) | \Psi_{QLAS}(\vec{\theta}) \rangle}, \quad (10)$$

where $\Psi_{QLAS}(\vec{\theta})$ is the HEA with the LASSCF wave function as the initial state (i.e. step 1 in Algorithm 1), and \hat{H}_{QLAS} is the Hamiltonian of the active space in the qubit basis. In addition to the increase in parameters needed to be optimized compared to HEA, the measurements naively scale $O(N_q^8)$ compared to $O(N_q^4)$. The increased measurement costs, however, can be further reduced with operator grouping and shot-frugal techniques, as described in Section III D.

Computational details

The ground state energies of the following chemical systems are computed: H_4 at two different geometries and square cyclobutadiene, where the simulations require qubits counts of 8 respectively. All molecular simulations with VQE and nuVQE (Section III. A. to C.) are noiseless and carried out with DI state preparation with Qiskit (version 0.46),⁵⁶ Aer state vector simulator (qiskit-aer version 0.11.1) and Limited-memory BFGS Bound(L-BFGS-B) optimizer⁵⁷ with *scipy*. The initial values of α_i and $\lambda_{i,j}$ are sampled from a distribution, $\text{Uniform}(-\epsilon, \epsilon)$, where $\epsilon = 0.1$ in our calculations. LASSCF calculations are performed with the *mrh*⁵⁸ package, and HF related calculations with *pyscf*.⁵⁹ To illustrate Pauli grouping and shot-frugal techniques to optimize the algorithm, we performed noiseless QASM simu-

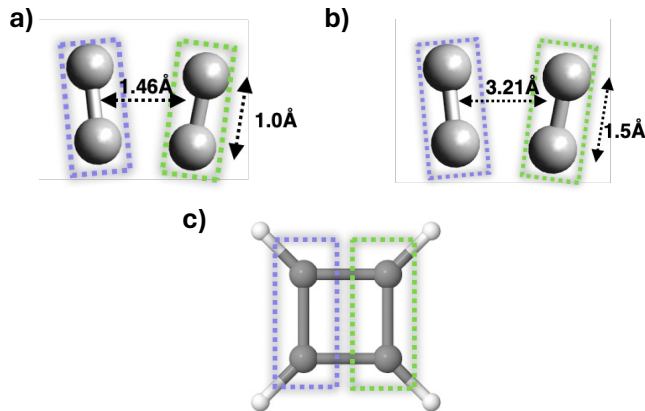


Figure 2: Systems studied in this work with purple and green boxes indicating the LASSCF fragments: **a)** two hydrogen molecules (intramolecular distance = 1.0 Å) separated by 1.46 Å (Geometry 1). **b)** two hydrogen molecules (intramolecular distance of 1.5 Å) separated by 3.21 Å (Geometry 2). **c)** square cyclobutadiene where all C-H bonds are 1.069 Å and C-C bonds are 1.456 Å.

lations with the QASM simulator from the Qiskit BasicAer module, as described in Section D. The corresponding basis sets, active spaces, and simulation details for each example are introduced in the respective sections.

III. Results and Discussions

Hardware-efficient ansatz comparison

Many forms of HEA exist due to the use of native quantum gates like rotation- y (R_y) gates and CNOT gates. Before discussing the nuVQE algorithm, we benchmark the performance and effectiveness of using the HEA as the trial wave function for VQE calculations using various initial states. We compare the performance of three widely-used ansatzes with R_y rotation gates and different connectivity, namely linear, full, and cascade (see Appendix A), for the H_4 system with Geometry 1 and minimal STO-3G basis set (8 qubits used). We also compare three initial states: all zero parameters, Hartree-Fock (HF), and LASSCF. For LASSCF, we choose an active space of $(2e, 2o)$ for each fragment (H_2). We carry out noiseless VQE calculations with the statevector simulator, and the data plotted are taken from the

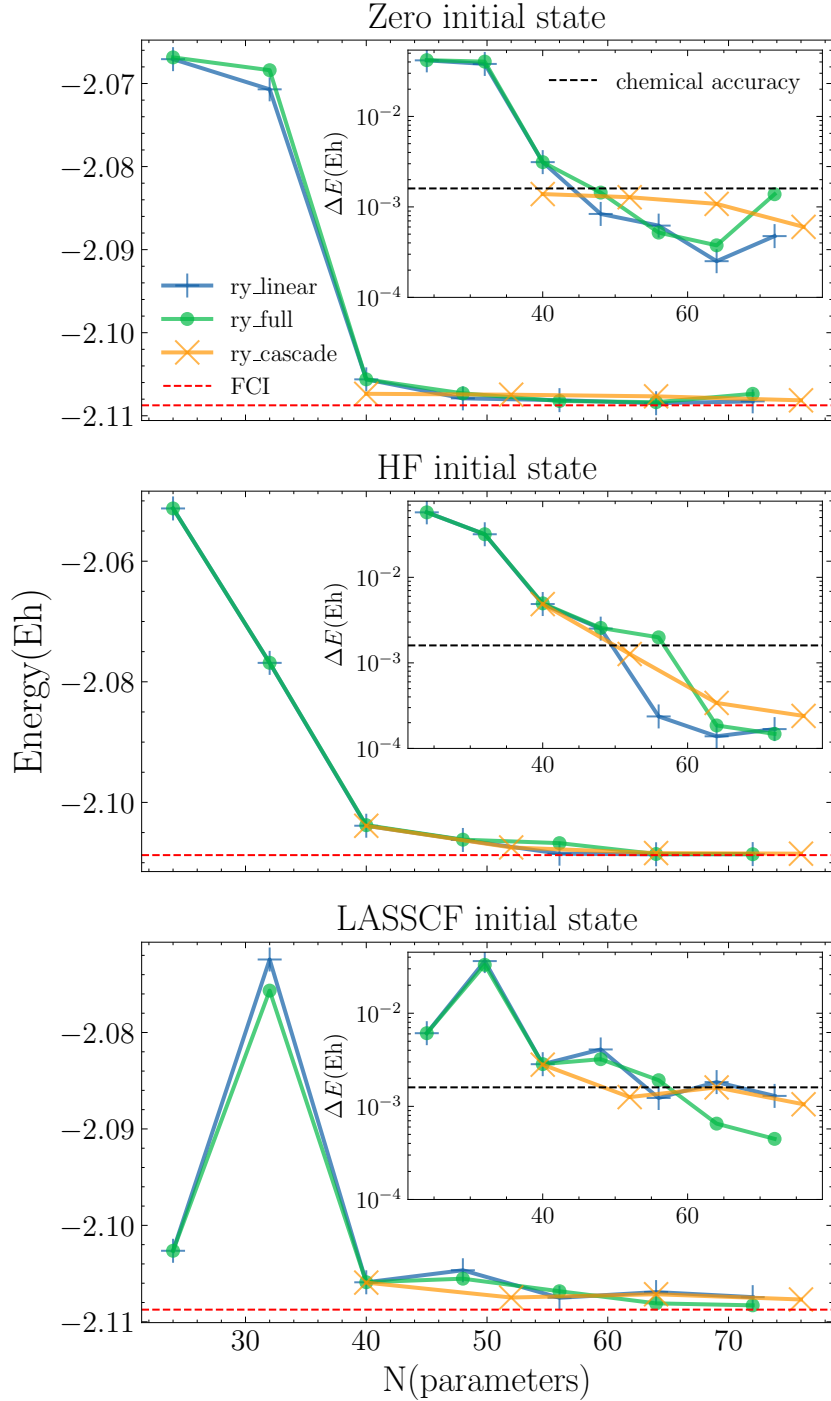


Figure 3: Performance benchmark of three hardware-efficient ansatzes: linear, full and cascade connectivity on system H_4 (Geometry 1) with minimal STO-3G basis set and increased number of layers (2-9 for ry_linear and ry_full, 2-5 for ry_cascade). Three different initial states: 0, Hartree-Fock (HF), and LASSCF are also being used to further compare the HEA.

lowest energy calculation from 1,000 independent runs.

Since each additional layer adds a different number of parameters to *Ry_cascade* compared to *Ry_linear* and *Ry_full*, we use the number of variational parameters in the ansatzes as x-axis and each point represents an additional layer for the respective ansatz. From Figure 3, we first observe that all but one energy values are above the chemical accuracy before 40 parameters, which corresponds to four repetitions of the linear and full connectivity, and one layer of the cascade connectivity. HEA thus fails to report accurate energies with short circuit depths (< 4 repetitions). When we increase the circuit depth by adding more layers, HEA agrees with FCI within chemical accuracy. However, the energy is not decreasing with more repetitions, although there are more variational parameters in the algorithm. Noticeably, the LASSCF initial state with two repetitions (24 variational parameters) outperforms the other two initial states and has significantly lower energy errors. We also observe that there is not one connectivity that substantially outperforms the others. Hence, we utilize *Ry_linear* as our choice of HEA for the rest of the results.

Single-point calculations

H_4 system

For the initial testing of LAS-nuVQE, we explored the two H_4 system illustrated in Figure 2 with a minimal STO-3G basis set and a Jordan-Wigner transformation.⁵¹ An active space of (2e, 2o) for each fragment is used corresponding to a total number of 8 qubits. We run 1,000 independent VQE calculations and 100 independent nuVQE calculations at all circuit repetitions (2 layers to 6 layers) with optimizer L-BFGS-B at each geometry. The plotted data corresponds to the lowest energy result. The total number of classical parameters to be optimized is 60 (24 for HEA and 36 from Jastrow operators).

As Figure 4 shows, at geometry 1, LASSCF is above chemical accuracy, indicating an approximation that is too drastic. LAS-nuVQE achieves chemical accuracy with only 2 layers of HEA, which translates to 24 single-qubit gates (SQGs) and 21 CNOT gates (< 50 total

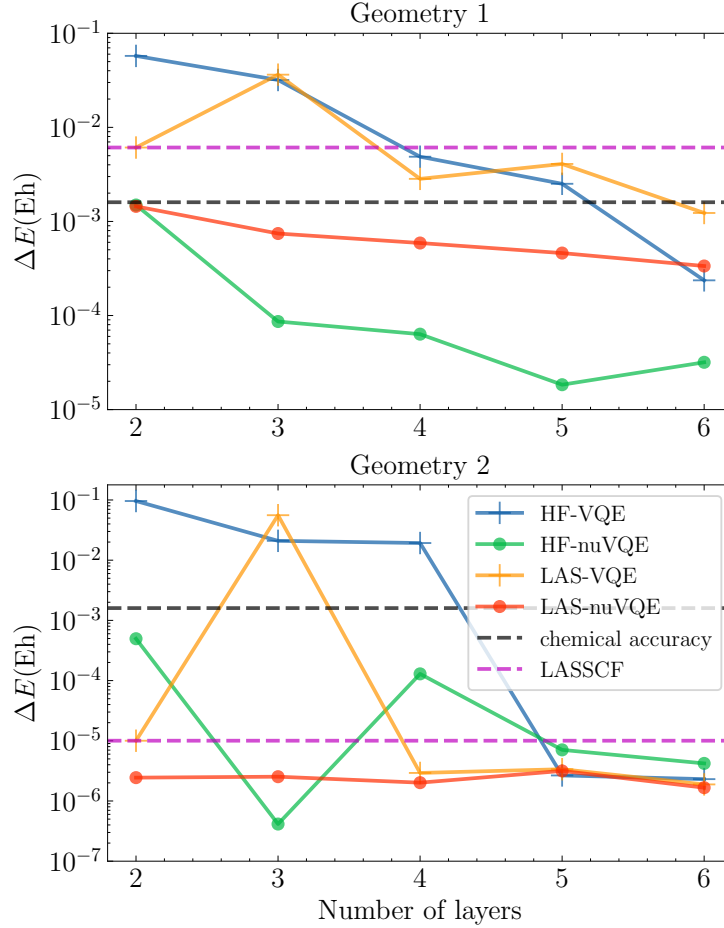


Figure 4: VQE and nuVQE results with HF and LASSCF initial states for two geometries of H_4 and minimal basis set STO-3G. x-axis is the number of circuit repetitions for HEA, and y-axis is the log scale of energy difference from full configuration interaction (FCI) reference.

number of gates). It illustrates that LAS-nuVQE can recover interfragment correlations and gives a more accurate energy. In addition, LAS-nuVQE is closer to the FCI reference at all circuit repetitions than LAS-VQE. Similar behavior is observed with the HF initial state as well. For geometry 2, LASSCF is a good approximation, indicated by the energy well below chemical accuracy. nuVQE is still able to improve LASSCF energies. Again, LAS-nuVQE outperforms the LAS-VQE counterparts at all circuit layers. This means that at the same number of HEA layers, LAS-nuVQE is more accurate than LAS-VQE. These test results encouraged us to explore more realistic systems.

Square Cyclobutadiene

Cyclobutadiene is an anti-aromatic and highly strained molecule. Its 1^1B_{1g} ground state has two degenerate singly occupied frontier orbitals and represents a challenge for single configuration methods.⁶⁰ We calculated this open-shell singlet ground-state at the square geometry, where the four carbon-carbon bonds are 1.456 Å, and the carbon-hydrogen bonds 1.069 Å. The chosen active space is (4e, 4o), which is further broken down into two (2e, 2o) fragments corresponding to a total number of 8 qubits. The cc-pvdz basis set⁶¹ was used. The results presented are taken from 1,000 independent VQE calculations and 100 independent nuVQE at all circuit repetitions (2 layers to 6 layers) with optimizer L-BFGS-B.

As Figure 5 (a) shows, LAS-nuVQE reaches chemical accuracy with 4 layers, which translates to 40 SQGs, 28 CNOT gates (< 70 total number of gates) and a total number of classical parameters of 76 (40 from HEA and 36 from Jastrow operators). The LAS-nuVQE energy is below the LAS-VQE value at all circuit repetitions. Noticeably, LAS-VQE never reaches chemical accuracy even with 6 repetitions, suggesting that one has to increase the circuit depth drastically to obtain energies comparable to the LAS-nuVQE results. In addition, we calculated the % of missing interfragment correlations recovered from LAS-nuVQE and LAS-VQE (Figure 5(b)) as a function of the number of layers for both methods as

$$p_0 = \frac{E_{LASSCF} - E_{LAS-nuVQE}}{E_{LASSCF} - E_{CASCI}}. \quad (11)$$

We notice that nuVQE recovers 95%+ of the interfragment correlation with 2 layers, and above 99.9% for 4 and above repetitions.

Spin-constrained calculations

One of the pitfalls of HEA is that it cannot preserve the total spin (\hat{S}^2) of the wave function, where the total spin operator can be measured with $\hat{S}^2 = \hat{S}_+\hat{S}_- + \hat{S}_z^2 + \hbar\hat{S}_z$. In the case

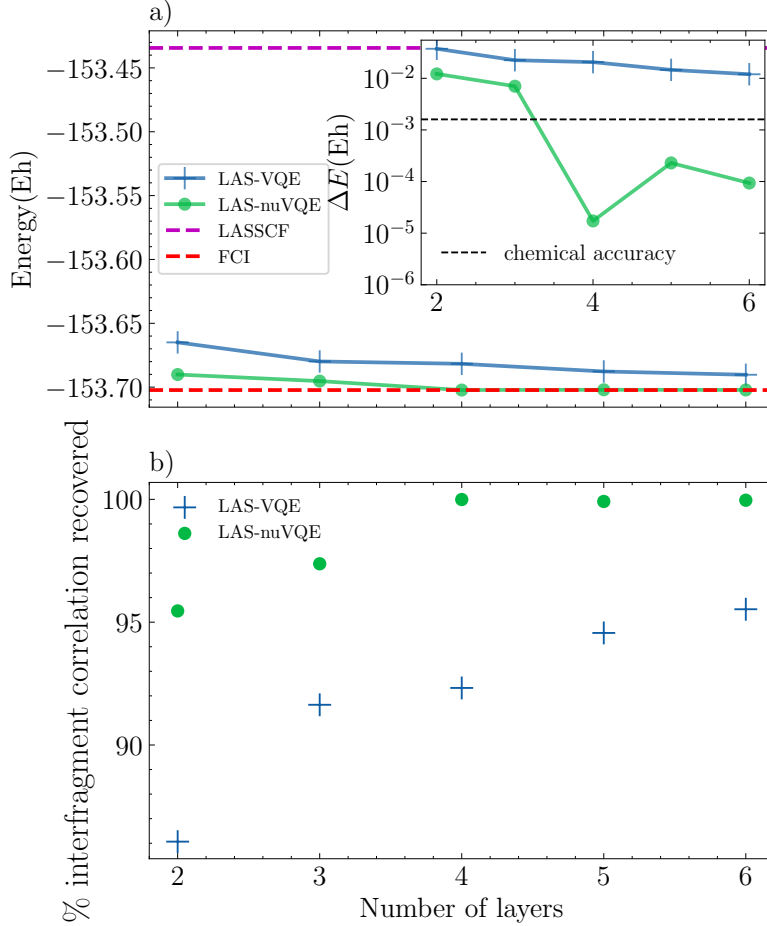


Figure 5: VQE and nuVQE comparison for square cyclobutadiene. **a)** plots the energy vs. the number of HEA layers, with inset’s y-axis being the log scale of the energy difference from CASCI reference. The bottom panel **b)** calculates the % of interfragment correlation recovered from LASSCF.

of square cyclobutadiene reported in Section III, the total spin of the wave function should be 0, while we observe spin contaminations ranging from 0.67 to 1.52 in all calculations as reported in Table 1. To perform meaningful chemical calculations with LAS-nuVQE, we implemented a spin penalty term in the energy optimization cost function,⁶²

$$E(\boldsymbol{\theta}) := L(\boldsymbol{\theta}) + \mu_C \left\langle \Psi_{QLAS}(\boldsymbol{\theta}) \left| (\hat{C} - c)^2 \right| \Psi_{QLAS}(\boldsymbol{\theta}) \right\rangle \quad (12)$$

where $L(\boldsymbol{\theta})$ is the energy calculated using eq (10), $\mu_C = 1$,⁶² \hat{C} is the total spin operator in this specific case, and c is the ideal spin state.

Table 1: Unconstrained LAS-VQE and LAS-nuVQE results for cyclobutadiene reported in Section B. Energy (in Hartree) corresponds to the points plotted in Figure 5. VQE is taken as the lowest energy result from 1000 independent runs, nuVQE is taken from 100 independent runs.

Method	Layer	Energy	Spin(\hat{S}^2)
Unconstrained LAS-VQE	2	-153.66495918	1.23278361
	3	-153.67988680	1.20112778
	4	-153.68172310	1.14305232
	5	-153.68772309	0.9311722
	6	-153.69030785	0.79768462
Unconstrained LAS-nuVQE	2	-153.69012437	1.15427599
	3	-153.69526760	0.67047731
	4	-153.70227735	0.99937762
	5	-153.70206538	1.51563038
	6	-153.70220104	1.06992523

Table 2: Spin-constrained LAS-VQE and LAS-nuVQE results for cyclobutadiene reported. Energy unit is in Hartree, and both VQE and nuVQE are taken as the lowest result among 50 calculations.

Method	Layer	Energy	Spin(\hat{S}^2)
Constrained LAS-VQE	2	-153.64195397	1.15821369e-09
	3	-153.64195398	2.34582602e-09
	4	-153.66371492	9.58401288e-05
	5	-153.66427448	3.31614262e-05
	6	-153.66417350	0.00056101
Constrained LAS-nuVQE	2	-153.68087791	5.94048096e-06
	3	-153.67765748	7.17730272e-05
	4	-153.67582877	0.00024698
	5	-153.69621423	0.00043989
	6	-153.66854958	0.00023403

As Table 2 shows, we have constrained the HEA to the correct spin state. For validation of the spin conservation, we run multiple independent runs and show the lowest energy results taken from 50 independent runs from both methods. We expect that with more optimization runs, we could achieve lower energies. Our results again have shown that at the same number of layers, LAS-nuVQE always improves on LAS-VQE results.

Mitigating measurement costs

So far, we have shown that LAS-nuVQE is effective in recovering correlations from LASSCF with small systems and is affordable to run with quantum resources available today. However, to tackle larger chemical systems in the future, we need to optimize the LAS-nuVQE algorithm, namely the measurement overhead, to make LAS-nuVQE affordable. The number of Pauli strings for the Hamiltonian operator scales naively as $O(N_q^4)$. The modified Pauli strings $J(\vec{\alpha}, \vec{\lambda})^\dagger H J(\vec{\alpha}, \vec{\lambda})$ could potentially scale up to $O(N_q^8)$ and the cost of $J(\vec{\alpha}, \vec{\lambda})^\dagger J(\vec{\alpha}, \vec{\lambda})$ is one due to only Pauli Z and I present in the formulation and that the strings all commute. Measurement optimization and efficiency are highly relevant in the NISQ era. To overcome the measurement costs of the nuVQE algorithm, we explored Pauli grouping and shot-frugal techniques to illustrate that the method could be further optimized. Other methods to mitigate measurement costs not investigated in this work include Majorana classical shadow,^{63,64} low-rank decomposition,⁶⁵⁻⁶⁷ and fluid Fermionic fragments (F^3).⁶⁸

Pauli grouping

For any quantum operators \hat{O} , after mapping to a qubit operator $\hat{O} = \sum_i c_i \hat{P}_i$, the expectation value of that operator can be expressed as the weighted sum of the measurements of Pauli strings with their respective coefficients

$$\begin{aligned} \langle \hat{O} \rangle &= \langle \Psi | \hat{O} | \Psi \rangle = \langle \Psi | \sum_i c_i \hat{P}_i | \Psi \rangle \\ &= \sum_i c_i \langle \Psi | \hat{P}_i | \Psi \rangle = \sum_i c_i \langle \hat{P}_i \rangle. \end{aligned} \tag{13}$$

For diagonal Pauli operators, the expectation value in the computational basis (I and Z) can be directly measured. For nondiagonal operators such as the X and Y Pauli operators, the corresponding matrices can go through a basis change to be further diagonalized. Pauli grouping is hence a commonly-used method to reduce the necessary number of evaluations on

Table 3: Comparison of the number of groups of Pauli operator after qubit-wise commuting (QWC) and fully commuting (FC) techniques for systems of H_2, H_4 , and cyclobutadiene (C_4H_4) with three different mapping schemes.

		H_2			H_4			C_4H_4		
Pauli operator		Original	QWC	FC	Original	QWC	FC	Original	QWC	FC
Jordan-Wigner	Hamiltonian	185	46	9	361	73	19	249	44	12
	JHJ	3147	185	29	5879	349	59	3147	44	12
	JJ	163	1	1	163	1	1	163	1	1
Bravyi-Kitaev	Hamiltonian	185	34	9	361	70	19	361	70	23
	JHJ	3472	137	27	6448	269	63	6442	70	23
	JJ	163	1	1	163	1	1	163	1	1
Parity	Hamiltonian	185	34	9	361	73	19	217	36	13
	JHJ	3376	143	27	6350	269	63	3372	143	32
	JJ	163	1	1	163	1	1	163	1	1

a quantum hardware. By gathering Pauli strings into groups of simultaneously diagonalizable strings (i.e. share the same eigenbasis), the expectation value for each group’s Pauli strings can be determined with a single measurement with a classical post-processing step.^{6,9} Two common partitions include qubit-wise commutativity (QWC)^{6,69} and full commutativity (FC).⁷⁰ In QWC, two Pauli strings commute if the matrices commute at each index, whereas in FC, the commutation rule is applied to the whole operator.

Finding the optimal Pauli partition is the same as solving a graph partition problem known as the minimum clique cover problem, which is NP hard.⁶⁹ We hence only focus on applying QWC and FC techniques and illustrate the savings in Table 3 for systems H_2 , H_4 , and C_4H_4 . The H_2 and H_4 Hamiltonians encompass the full system, whereas C_4H_4 only includes the active space. We investigated three mapping schemes, Jordan-Wigner,⁵¹ Bravyi-Kitaev,⁷¹ and Parity⁷² for three operators: Hamiltonian (H), $J(\vec{\alpha}, \vec{\lambda})^\dagger H J(\vec{\alpha}, \vec{\lambda})$, and $J(\vec{\alpha}, \vec{\lambda})^\dagger J(\vec{\alpha}, \vec{\lambda})$ respectively. Across three mapping schemes, the measuring costs of the Hamiltonian operator is reduced by a factor of $\sim 4 - 21$ and $J(\vec{\alpha}, \vec{\lambda})^\dagger H J(\vec{\alpha}, \vec{\lambda})$ is reduced by a factor of $\sim 17 - 280$, which brings the total increased cost down to as little as a factor of 3. It shows that despite nuVQE introducing considerable measurement overhead, it can be

efficiently mitigated with Pauli grouping techniques, which have already been implemented in various hardware platforms.

Shot-frugal techniques

As previously discussed, the expectation value of a quantum operator is usually taken as the weighted sum of measured Pauli strings according to eq (13). The terms with a larger coefficient ‘contribute’ more to the final numerical expression and their accuracy might be more important. When measuring an expectation value with a limited number of shots, various strategies—often referred to as shot-frugal techniques—have been developed to optimize shot distribution and achieve high accuracy while minimizing resource usage.^{73,74} In this work, we leverage such strategies to reduce the computational cost associated with evaluating $J(\vec{\alpha}, \vec{\lambda})^\dagger H J(\vec{\alpha}, \vec{\lambda})$.

We explore three techniques: uniform deterministic sampling (UDS), weighted deterministic sampling (WDS), and weighted random sampling (WRS) and shows results with both the Hamiltonian and $J(\vec{\alpha}, \vec{\lambda})^\dagger H J(\vec{\alpha}, \vec{\lambda})$ operators respectively in Figure 6 and 7.

In UDS, the number of total shots (s_{tot}) is divided equally among N terms. In WDS, the number of shots is allocated deterministically proportional to the magnitude of the coefficients. In WRS, the number of shots is sampled from a multinomial probability distribution of which the probability (p_i) of measuring a given \hat{P}_i is proportional to the magnitude of the coefficient: $p_i = \frac{|c_i|}{M}$, where c_i is the coefficient and M is the sum of the coefficient. The

variances can be expressed as the following:

$$\text{Var}(\widehat{E}_{UDS}) = \frac{N}{s_{tot}} \sum_{i=1}^N |c_i|^2 \sigma_i^2 \quad (14)$$

$$\text{Var}(\widehat{E}_{WDS}) = \frac{M}{s_{tot}} \sum_{i=1}^N |c_i| \sigma_i^2 \quad (15)$$

$$\begin{aligned} \text{Var}(\widehat{E}_{WRS}) &= \frac{M}{s_{tot}} \sum_{i=1}^N |c_i| \sigma_i^2 \\ &+ \frac{s_{rand} M}{s_{tot}^2} \sum_{i=1}^N |c_i| \langle \hat{P}_i \rangle^2 - \frac{s_{rand} \langle \hat{O} \rangle^2}{s_{tot}^2} \end{aligned} \quad (16)$$

where σ_i is $\langle \hat{P}_i^2 \rangle - \langle \hat{P}_i \rangle^2$, s_{rand} is the random number of shots drawn from the multinomial distribution.

To showcase the shot-frugal techniques, we start with a converged VQE calculation and nuVQE calculation with UCCSD ansatz for the H_2 system and 6-31G basis set, and measure the expectation value of the Hamiltonian and $J(\vec{\alpha}, \vec{\lambda})^\dagger H J(\vec{\alpha}, \vec{\lambda})$ respectively. We use the statevector to calculate the two expectation values exactly. For each method (no shot-frugal, UDS, WDS, WRS), we run 5 independent calculations with the QASM simulation from Qiskit BasicAer module. We calculate the sample mean and take the energy difference from the exact value in Figure 6 and 7. We also calculate the standard error as $SEM = \frac{1}{\sqrt{n}} \sqrt{\frac{1}{n} \sum Var_i}$ where n is the number of runs and plot as error bars in the left panels of the two figures.

As Figure 6 right panel shows, all three shot-frugal techniques achieve a lower error with a small number of shots (10^2), and UDS and WDS achieve 1-2 orders of magnitude higher accuracy compared to direct QASM measurement with $10^4 - 10^6$ number of shots. It might require the QASM measurements to go even further with the number of shots, compared to the aforementioned two techniques, to obtain a similar error magnitude. Similarly in Figure 7 right panel, for operator $J(\vec{\alpha}, \vec{\lambda})^\dagger H J(\vec{\alpha}, \vec{\lambda})$, we observe that WDS can achieve higher accuracy with low magnitude of shots (10^1), and WDS and WRS reaches 1-2 magnitudes higher of accuracy with 10^2 of shots. WRS shows a more significant advantage with an increased

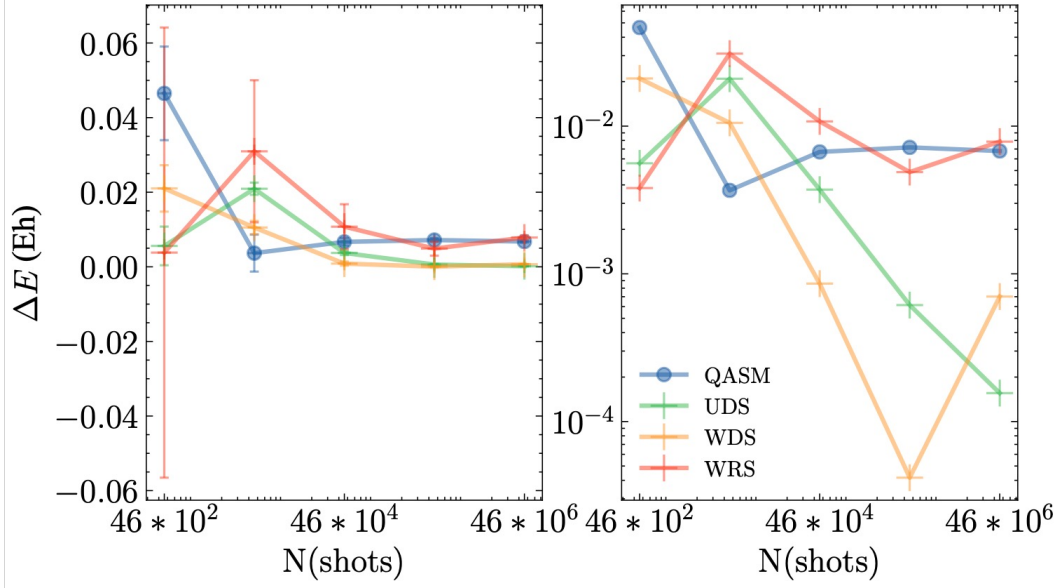


Figure 6: Shot-frugal technique comparison for the Hamiltonian operator with the H_2 system at equilibrium and with the 6-31G basis set.

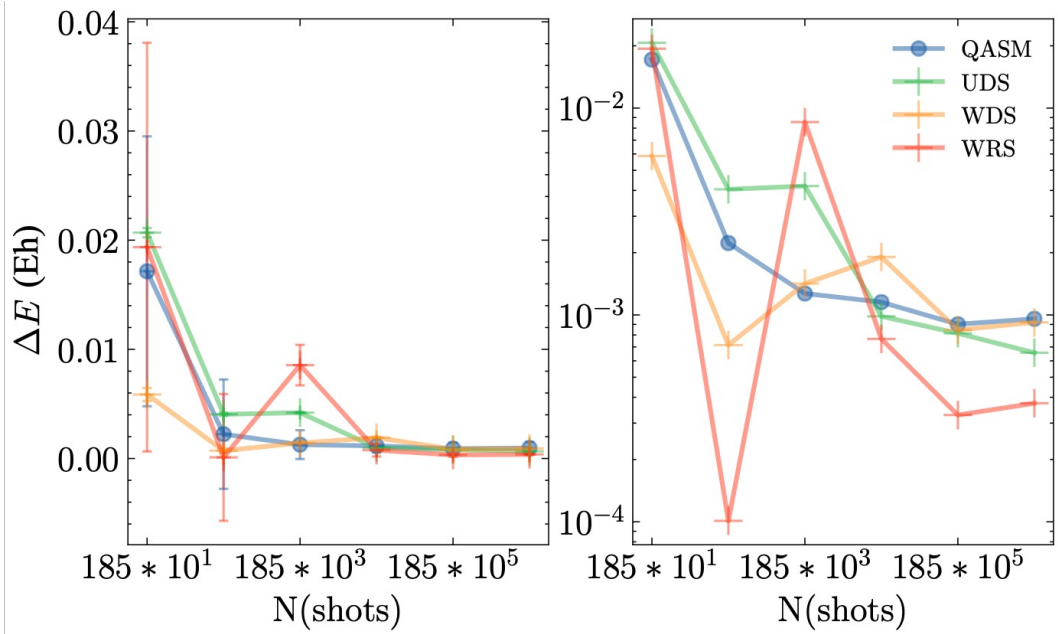


Figure 7: Shot-frugal technique comparison for the $J(\vec{\alpha}, \vec{\lambda})^\dagger H J(\vec{\alpha}, \vec{\lambda})$ operator with the H_2 system at equilibrium and 6-31G basis set.

number of shots $10^4 - 10^6$. Although not one shot-frugal technique is shown to *always* outperform direct QASM measurements, we see that it oftentimes is more accurate when having extremely limited of shots, and an overall smaller error magnitude with more shots,

which would require direct QASM measurement even more number of magnitude of shots to achieve. Notice our results are limited to 5 runs, and the performance of the shot-frugal techniques can change when we have more experiments. It serves as a demonstration that when measuring $J(\vec{\alpha}, \vec{\lambda})^\dagger H J(\vec{\alpha}, \vec{\lambda})$, one might require less number of shots with the help of shot-frugal techniques.

Shot-frugal techniques with qubit-wise grouped Paulis

To mimic hardware behavior, we further explore the aforementioned three shot-frugal techniques (UDS, WDS, WRS) with QWC grouped Paulis for the $J(\vec{\alpha}, \vec{\lambda})^\dagger H J(\vec{\alpha}, \vec{\lambda})$ operator.

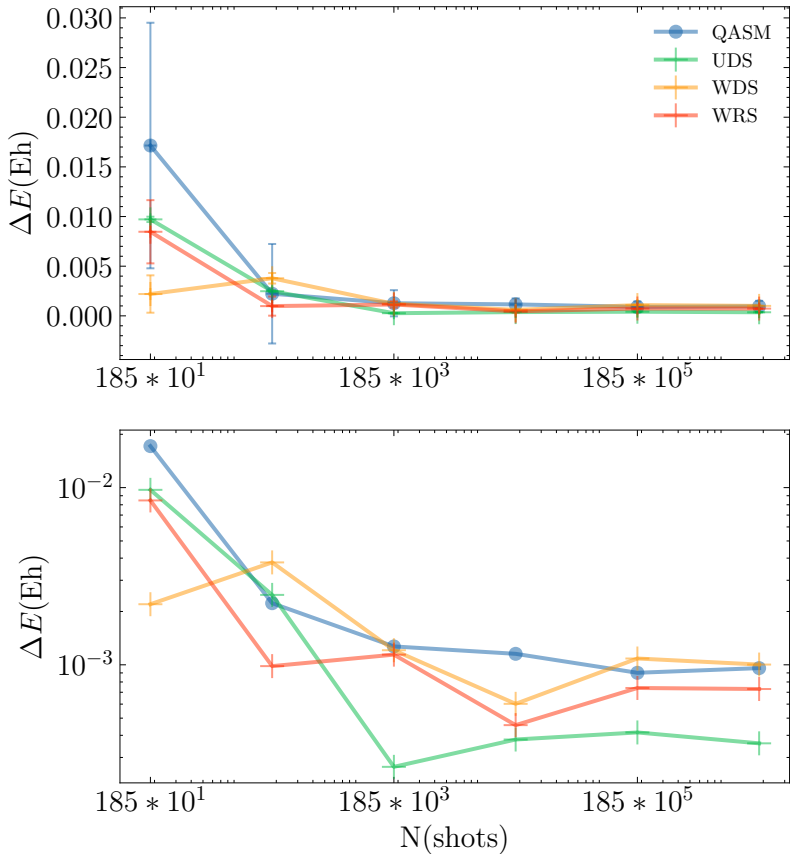


Figure 8: Shot-frugal technique with qubit-wise grouped Paulis for the $J(\vec{\alpha}, \vec{\lambda})^\dagger H J(\vec{\alpha}, \vec{\lambda})$ operator with the H_2 system at equilibrium and with the 6-31G basis set.

From Fig. 8, we see that with a small magnitude of shots (10^1), all three shot-frugal techniques report more accurate energies compared to QASM. WRS seems to outperform

QASM measurements at all number of shots, whereas UDS reports a smaller magnitude of errors with 10^3 and above magnitude of shots. WDS seems to perform similarly to QASM with 10^1 and 10^4 magnitudes being the only two points to report a more accurate energy value compared to QASM. With results in Figure 8, we illustrate that one can further combine the mitigation techniques and mitigate measurement costs for the LAS-nuVQE method.

Scalability

We have explored and provided strategies to optimize the LAS-nuVQE algorithms for shorter runtime (by mitigation of measurement costs) and achieving accurate energies with affordable quantum resources. In this section, we further provide resource comparison for each methodological development in this work in the form of wall clock time.⁷⁵ Specifically, we compare the time required for one iteration of VQE for vanilla HEA (HEA in the figure), HEA with nuVQE (nuVQE in the figure), and HEA with nuVQE and measurement mitigation. We follow a similar formalization for wall clock estimation,⁷⁵ that time needed for one query can be described by $T_{prepare} + T_{sample} + T_{switch} + T_{cloud}$. $T_{prepare}$ is an add-on here to incorporate gate costs and it is the time it takes to initialize a circuit. T_{sample} describes the time for sampling circuits on quantum processors. T_{switch} is the time for the overhead in switching between different circuits, and T_{cloud} describes latency in communication.

For numerical estimations, $T_{prepare} = g * p$, where g is the total number of gates and p is the rate of executing gates. $T_{sample} = M/s$, where M is the number of measurements and s is the sampling rate. $T_{switch} = r * c$, which r represents the overhead in readying and c is the number of different circuits. Lastly, $T_{cloud} = l * c/b$, where l is the round-trip time for network and b is the number of circuits sent. For superconducting platform, we set $s = 10^5 Hz$, $r = 0.1s$, and $l = 4.0s$, and average gate execution time to be $p = 660ns$.⁷⁶ For trapped ion/neutral atom platforms, we combine $T_{prepare}$ and T_{sample} to M/s and estimate the shot acquisition time to 200ms ($s = 5Hz$), which includes the time for circuit initialization, circuit execution, and one single measurement.⁷⁴ The overhead in reading, $r = 0.025s$,⁷⁴ and we

assume the same $l = 4.0s$.

To carry out calculations for any chemical systems, knowing the number of layers or parameters needed for any HEA to achieve chemical accuracy is almost impossible. Therefore, we assume the number of layers needed equals to the number of qubits: $N_l = N_q$. For HEAs, the single qubit gates scale as $N_q * (1 + N_l)$. Since nuVQE achieves chemical accuracy faster than vanilla HEA-only VQEs, we assume that one Jastrow parameter, which scales as $\frac{1}{2}N_q * (N_q + 1)$, can save one SQG. Based on the performance of shot frugal techniques, we assume that the number of shots needed is 2 orders of magnitude less. We first obtained

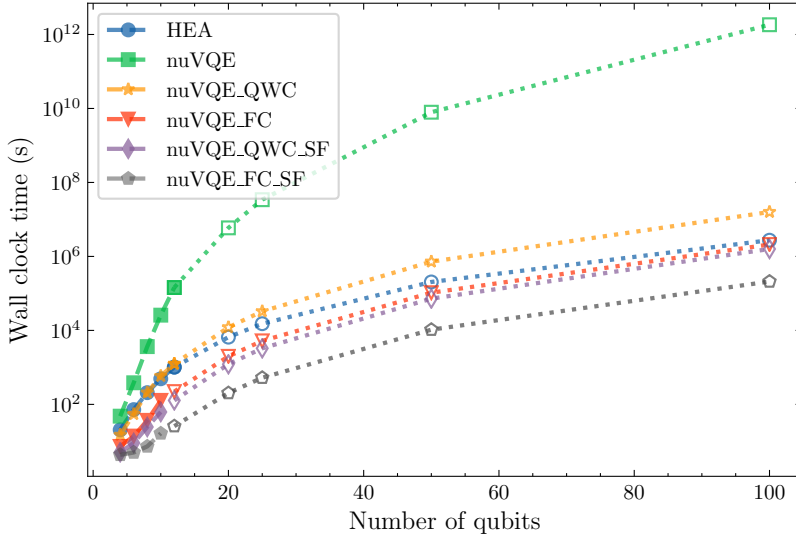


Figure 9: Wall clock estimation for one query for each method on a superconducting platform for hydrogen chains. Hollow markers indicate the extrapolated points.

the number of Paulis and grouped Paulis for hydrogen chains H_2, H_3, H_4, H_5, H_6 (4, 6, 8, 10, 12 qubits respectively). This number (hereafter h) also represents the number of unique circuits for the measurements. We then fit $\ln(h)$ vs. $\ln(N_q)$ to a straight line then derive constants a and p such that $h(N_q) \approx a n^p$. We then use this relationship to extrapolate h at larger values of N_q , specifically 20, 25, 50, and 100 qubits. We specifically compare six methods: ‘HEA’ represents the well-known vanilla VQE with HEA; ‘nuVQE’ means HEA with VQE; ‘QWC’ indicates qubit-wise grouping is utilized; ‘FC’ means fully-commuting grouping is used; and ‘SF’ is short for shot-frugal.

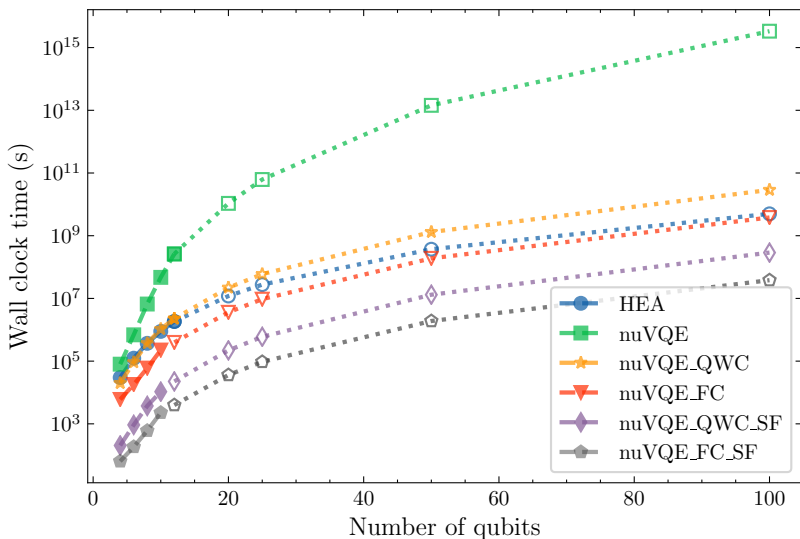


Figure 10: Wall clock estimation for one query for each method on a neutral atom/trapped ion platform for hydrogen chains. Hollow markers indicate the extrapolated points.

As Fig. 9 and Fig. 10 both show, untreated nuVQE quickly becomes unrealistic as the number of qubits increases. At 100 qubits, one query of nuVQE will take about 31,688 years for the superconducting platform and 31,688,764 years for the natural atom/trapped ion platform. HEA will take less than 280 hours on superconducting platforms and 32 years on trapped ion/neutral atom platform. nuVQE with shot-frugal techniques and grouped Paulis can further reduce the time costs down to < 28 hours on superconducting platforms. In cases where fully-commuting grouping is intractable, qubit-wise grouping and shot-frugal techniques for nuVQE still give a clock time scaling less than HEA, showing its promise in running 100-qubit calculations with realistic wall clock and resources.

IV. Conclusion

In this paper, we have explored the nuVQE method with LASSCF as the initial state. LAS-nuVQE has shown that it can recover interfragment correlations and achieve chemical accuracies with limited quantum resources (<70 total gates) for small systems like H_4 and C_4H_4 . To carry out meaningful multireference chemical calculations in the future, we

first noted the pitfall of HEA and devised the addition of penalty terms to allow for spin-conversation in the ansatz. Our results have shown that we can correctly preserve the spin and it allows one to study more complex chemical properties with HEA or HEA-related methods. Then, to optimize the method further to enable large chemical calculations, we explored Pauli grouping and shot-frugal techniques. We illustrated that one can significantly reduce measurement costs with grouping and shot-frugal techniques to report a more accurate energy expectation value. Additionally, we provided resource estimation in the form of wall clock time for the methods we explored, showing that with measurement mitigation techniques, LAS-nuVQE remains a competitive candidate for tackling chemical calculations with quantum algorithms.

There are several future directions for further investigation in this area. For instance, it would be valuable to explore methods of loading the LASSCF wave function in a way that strictly preserves spin symmetry, thereby maintaining accurate electronic state representations throughout variational optimization. Additionally, examining alternative connectivity patterns for HEA could potential provide deeper insights into achieving faster convergence or improved accuracy by taking advantage of the available qubit connectivity in near-term quantum devices. Another direction involves adopting the local unitary cluter Jastrow (LUCJ) ansatz for capturing electron correlation as another post-LASSCF method. LUCJ is formulated as an approximation to the general unitary cluster Jastrow (UCJ) ansatz, it retains a strong chemical motivation and may offer a cost-effective compromise between accuracy and resource requirements. Furthermore, investigating the performance of LAS-nuVQE with noise models and its performance when combined with error mitigation techniques could suggest whether it exhibits robust noise-resilient features when compared with more conventional ansatz like UCCSD. Such study would be helpful to understand the potential of LAS-nuVQE for practical quantum simulations in NISQ era for reliable electronic structure calculations.

Appendix A: Hardware-efficient ansatz

Here we show the HEA with three different connectivities that we explored in this work.

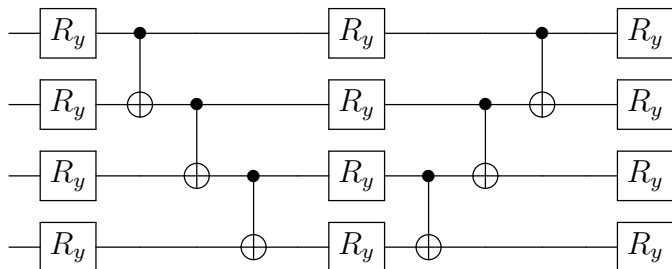


Figure 11: Cascade connectivity with 4 qubits and 1 layer

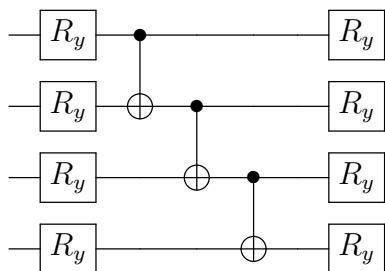


Figure 12: Linear connectivity with 4 qubits and 1 layer

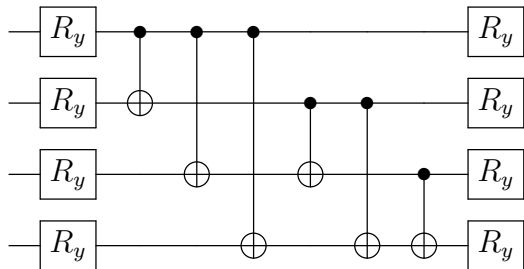


Figure 13: Full connectivity with 4 qubits and 1 layer

Acknowledgement

The authors thank Dr. Mario Motta, Dr. Kevin Sung, and Dr. Leon Otis for their helpful discussions and feedback on this work. This work was supported by the U.S. Department of Energy, Office of Science, National Quantum Information Science Research Centers and

partially by NSF QuBBE Quantum Leap Challenge Institute (NSF OMA-2121044). The authors thank the Research Computing Center at the University of Chicago for the computing resources.

Supporting Information Available

The supporting information contains the absolute energies for hardware-efficient ansatzes comparison, the absolute energies for single-point calculations of two geometries of H_4 , expectation value measurement data for shot-frugal techniques, and data used for wall clock time calculation.

Data and Code Availability

The data that support the findings of this study are available within the article and in the supporting information. The code is available at <https://github.com/joannaqw/LAS-nuVQE>.

References

- (1) McArdle, S.; Endo, S.; Aspuru-Guzik, A.; Benjamin, S. C.; Yuan, X. Quantum computational chemistry. *Reviews of Modern Physics* **2020**, *92*, 015003.
- (2) Bauer, B.; Bravyi, S.; Motta, M.; Chan, G. K.-L. Quantum Algorithms for Quantum Chemistry and Quantum Materials Science. *Chemical Reviews* **2020**, *120*, 12685–12717.
- (3) Cao, Y.; Romero, J.; Olson, J. P.; Degroote, M.; Johnson, P. D.; Kieferová, M.; Kivlichan, I. D.; Menke, T.; Peropadre, B.; Sawaya, N. P. D.; Sim, S.; Veis, L.; Aspuru-Guzik, A. Quantum Chemistry in the Age of Quantum Computing. *Chemical Reviews* **2019**, *119*, 10856–10915.

- (4) Head-Marsden, K.; Flick, J.; Ciccarino, C. J.; Narang, P. Quantum Information and Algorithms for Correlated Quantum Matter. *Chemical Reviews* **2021**, *121*, 3061–3120.
- (5) Preskill, J. Quantum Computing in the NISQ era and beyond. *Quantum* **2018**, *2*, 79.
- (6) Kandala, A.; Mezzacapo, A.; Temme, K.; Takita, M.; Brink, M.; Chow, J. M.; Gambetta, J. M. Hardware-efficient variational quantum eigensolver for small molecules and quantum magnets. *Nature* **2017**, *549*, 242–246.
- (7) Peruzzo, A.; McClean, J.; Shadbolt, P.; Yung, M.-H.; Zhou, X.-Q.; Love, P. J.; Aspuru-Guzik, A.; O’Brien, J. L. A variational eigenvalue solver on a photonic quantum processor. *Nature Communications* **2014**, *5*.
- (8) Tilly, J.; Chen, H.; Cao, S.; Picozzi, D.; Setia, K.; Li, Y.; Grant, E.; Wossnig, L.; Rungger, I.; Booth, G. H.; Tennyson, J. The Variational Quantum Eigensolver: A review of methods and best practices. *Physics Reports* **2022**, *986*, 1–128, The Variational Quantum Eigensolver: a review of methods and best practices.
- (9) McClean, J. R.; Romero, J.; Babbush, R.; Aspuru-Guzik, A. The theory of variational hybrid quantum-classical algorithms. *New Journal of Physics* **2016**, *18*, 023023.
- (10) Taube, A. G.; Bartlett, R. J. New perspectives on unitary coupled-cluster theory. *International Journal of Quantum Chemistry* **2006**, *106*, 3393–3401.
- (11) Poulin, D.; Hastings, M. B.; Wecker, D.; Wiebe, N.; Doherty, A. C.; Troyer, M. The Trotter Step Size Required for Accurate Quantum Simulation of Quantum Chemistry. 2014; <https://arxiv.org/abs/1406.4920>.
- (12) Moll, N. et al. Quantum optimization using variational algorithms on near-term quantum devices. *Quantum Science and Technology* **2018**, *3*, 030503.
- (13) D’Cunha, R.; Crawford, T. D.; Motta, M.; Rice, J. E. Challenges in the Use of Quantum

- Computing Hardware-Efficient Ansätze in Electronic Structure Theory. *The Journal of Physical Chemistry A* **2023**, *127*, 3437–3448.
- (14) Ryabinkin, I. G.; Lang, R. A.; Genin, S. N.; Izmaylov, A. F. Iterative Qubit Coupled Cluster Approach with Efficient Screening of Generators. *Journal of Chemical Theory and Computation* **2020**, *16*, 1055–1063.
- (15) Lee, J.; Huggins, W. J.; Head-Gordon, M.; Whaley, K. B. Generalized Unitary Coupled Cluster Wave functions for Quantum Computation. *Journal of Chemical Theory and Computation* **2019**, *15*, 311–324.
- (16) Grimsley, H. R.; Economou, S. E.; Barnes, E.; Mayhall, N. J. An adaptive variational algorithm for exact molecular simulations on a quantum computer. *Nature Communications* **2019**, *10*, 3007.
- (17) Tang, H. L.; Shkolnikov, V.; Barron, G. S.; Grimsley, H. R.; Mayhall, N. J.; Barnes, E.; Economou, S. E. Qubit-ADAPT-VQE: An Adaptive Algorithm for Constructing Hardware-Efficient Ansätze on a Quantum Processor. *PRX Quantum* **2021**, *2*, 020310.
- (18) Fedorov, D. A.; Alexeev, Y.; Gray, S. K.; Otten, M. Unitary Selective Coupled-Cluster Method. *Quantum* **2022**, *6*, 703.
- (19) Mitra, A.; D’Cunha, R.; Wang, Q.; Hermes, M. R.; Alexeev, Y.; Gray, S. K.; Otten, M.; Gagliardi, L. The Localized Active Space Method with Unitary Selective Coupled Cluster. *Journal of Chemical Theory and Computation* **2024**, *20*, 7865–7875.
- (20) Matsuzawa, Y.; Kurashige, Y. Jastrow-type Decomposition in Quantum Chemistry for Low-Depth Quantum Circuits. *Journal of Chemical Theory and Computation* **2020**, *16*, 944–952.

- (21) Motta, M.; Sung, K. J.; Whaley, K. B.; Head-Gordon, M.; Shee, J. Bridging physical intuition and hardware efficiency for correlated electronic states: the local unitary cluster Jastrow ansatz for electronic structure. *Chemical Science* **2023**, *14*, 11213–11227.
- (22) Mazzola, G.; Ollitrault, P. J.; Barkoutsos, P. K.; Tavernelli, I. Nonunitary Operations for Ground-State Calculations in Near-Term Quantum Computers. *Physical Review Letters* **2019**, *123*, 130501.
- (23) Benfenati, F.; Mazzola, G.; Capecchi, C.; Barkoutsos, P. K.; Ollitrault, P. J.; Tavernelli, I.; Guidoni, L. Improved Accuracy on Noisy Devices by Nonunitary Variational Quantum Eigensolver for Chemistry Applications. *Journal of Chemical Theory and Computation* **2021**, *17*, 3946–3954.
- (24) Gagliardi, L.; Truhlar, D. G.; Li Manni, G.; Carlson, R. K.; Hoyer, C. E.; Bao, J. L. Multiconfiguration Pair-Density Functional Theory: A New Way To Treat Strongly Correlated Systems. *Accounts of Chemical Research* **2017**, *50*, 66–73.
- (25) Hermes, M. R.; Gagliardi, L. Multiconfigurational Self-Consistent Field Theory with Density Matrix Embedding: The Localized Active Space Self-Consistent Field Method. *Journal of Chemical Theory and Computation* **2019**, *15*, 972–986.
- (26) Hermes, M. R.; Pandharkar, R.; Gagliardi, L. Variational Localized Active Space Self-Consistent Field Method. *Journal of Chemical Theory and Computation* **2020**, *16*, 4923–4937.
- (27) Jiménez-Hoyos, C. A.; Scuseria, G. E. Cluster-based mean-field and perturbative description of strongly correlated fermion systems: Application to the one- and two-dimensional Hubbard model. *Physical Review B* **2015**, *92*, 085101.
- (28) Roos, B. O.; Taylor, P. R.; Sigbahn, P. E. A complete active space SCF method

- (CASSCF) using a density matrix formulated super-CI approach. *Chemical Physics* **1980**, *48*, 157–173.
- (29) Pandharkar, R.; Hermes, M. R.; Cramer, C. J.; Gagliardi, L. Spin-State Ordering in Metal-Based Compounds Using the Localized Active Space Self-Consistent Field Method. *The Journal of Physical Chemistry Letters* **2019**, *10*, 5507–5513.
- (30) Wang, Q.; Agarawal, V.; Hermes, M. R.; Motta, M.; Rice, J. E.; Jones, G. O.; Gagliardi, L. Distinguishing homolytic vs heterolytic bond dissociation of phenylsulfonium cations with localized active space methods. *The Journal of Chemical Physics* **2024**, *161*, 014106.
- (31) Abraham, V.; Mayhall, N. J. Selected Configuration Interaction in a Basis of Cluster State Tensor Products. *Journal of Chemical Theory and Computation* **2020**, *16*, 6098–6113.
- (32) Jiménez-Hoyos, C. A.; Scuseria, G. E. Cluster-based mean-field and perturbative description of strongly correlated fermion systems: Application to the one- and two-dimensional Hubbard model. *Physical Review B* **2015**, *92*, 085101.
- (33) Papastathopoulos-Katsaros, A.; Jiménez-Hoyos, C. A.; Henderson, T. M.; Scuseria, G. E. Coupled Cluster and Perturbation Theories Based on a Cluster Mean-Field Reference Applied to Strongly Correlated Spin Systems. *Journal of Chemical Theory and Computation* **2022**, *18*, 4293–4303.
- (34) Wang, Q.; Duan, M.; Xu, E.; Zou, J.; Li, S. Describing Strong Correlation with Block-Correlated Coupled Cluster Theory. *The Journal of Physical Chemistry Letters* **2020**, *11*, 7536–7543.
- (35) Otten, M.; Hermes, M. R.; Pandharkar, R.; Alexeev, Y.; Gray, S. K.; Gagliardi, L. Localized Quantum Chemistry on Quantum Computers. *Journal of Chemical Theory and Computation* **2022**, *18*, 7205–7217.

- (36) Buenker, R. J.; Peyerimhoff, S. D. Individualized configuration selection in CI calculations with subsequent energy extrapolation. *Theoretica chimica acta* **1974**, *35*, 33–58.
- (37) Buenker, R. J.; Peyerimhoff, S. D.; Butscher, W. Applicability of the multi-reference double-excitation CI (MRD-CI) method to the calculation of electronic wavefunctions and comparison with related techniques. *Molecular Physics* **1978**, *35*, 771–791.
- (38) Olsen, J.; Roos, B. O.; Jørgensen, P.; Jensen, H. J. A. Determinant based configuration interaction algorithms for complete and restricted configuration interaction spaces. *The Journal of Chemical Physics* **1988**, *89*, 2185–2192.
- (39) Ma, D.; Li Manni, G.; Gagliardi, L. The generalized active space concept in multiconfigurational self-consistent field methods. *The Journal of Chemical Physics* **2011**, *135*, 044128.
- (40) Vogiatzis, K. D.; Li Manni, G.; Stoneburner, S. J.; Ma, D.; Gagliardi, L. Systematic Expansion of Active Spaces beyond the CASSCF Limit: A GASSCF/SplitGAS Benchmark Study. *Journal of Chemical Theory and Computation* **2015**, *11*, 3010–3021.
- (41) Odoh, S. O.; Manni, G. L.; Carlson, R. K.; Truhlar, D. G.; Gagliardi, L. Separated-pair approximation and separated-pair pair-density functional theory. *Chemical Science* **2016**, *7*, 2399–2413.
- (42) Malmqvist, P. A.; Rendell, A.; Roos, B. O. The restricted active space self-consistent-field method, implemented with a split graph unitary group approach. *The Journal of Physical Chemistry* **1990**, *94*, 5477–5482.
- (43) Olsen, J.; Roos, B. O.; Jørgensen, P.; Jensen, H. J. A. Determinant based configuration interaction algorithms for complete and restricted configuration interaction spaces. *The Journal of Chemical Physics* **1988**, *89*, 2185–2192.

- (44) Chan, G. K.-L.; Zgid, D. In *Chapter 7 The Density Matrix Renormalization Group in Quantum Chemistry*; Wheeler, R. A., Ed.; Annual Reports in Computational Chemistry; Elsevier, 2009; Vol. 5; pp 149–162.
- (45) Marti, K. H.; Reiher, M. The Density Matrix Renormalization Group Algorithm in Quantum Chemistry. *Zeitschrift für Physikalische Chemie* **2010**, *224*, 583–599.
- (46) Yanai, T.; Kurashige, Y.; Mizukami, W.; Chalupský, J.; Lan, T. N.; Saitow, M. Density matrix renormalization group for ab initio Calculations and associated dynamic correlation methods: A review of theory and applications. *International Journal of Quantum Chemistry* **2015**, *115*, 283–299.
- (47) Olivares-Amaya, R.; Hu, W.; Nakatani, N.; Sharma, S.; Yang, J.; Chan, G. K.-L. The ab-initio density matrix renormalization group in practice. *The Journal of Chemical Physics* **2015**, *142*, 034102.
- (48) Chan, G. K.-L.; Keselman, A.; Nakatani, N.; Li, Z.; White, S. R. Matrix product operators, matrix product states, and ab initio density matrix renormalization group algorithms. *The Journal of Chemical Physics* **2016**, *145*, 014102.
- (49) Zgid, D.; Nooijen, M. The density matrix renormalization group self-consistent field method: Orbital optimization with the density matrix renormalization group method in the active space. *The Journal of Chemical Physics* **2008**, *128*, 144116.
- (50) Ghosh, D.; Hachmann, J.; Yanai, T.; Chan, G. K.-L. Orbital optimization in the density matrix renormalization group, with applications to polyenes and β -carotene. *The Journal of Chemical Physics* **2008**, *128*, 144117.
- (51) Fradkin, E. Jordan-Wigner transformation for quantum-spin systems in two dimensions and fractional statistics. *Physical Review Letters* **1989**, *63*, 322–325.

- (52) D’Cunha, R.; Otten, M.; Hermes, M. R.; Gagliardi, L.; Gray, S. K. State Preparation in Quantum Algorithms for Fragment-Based Quantum Chemistry. *Journal of Chemical Theory and Computation* **2024**, *20*, 3121–3130.
- (53) Lin, S.-H.; Dilip, R.; Green, A. G.; Smith, A.; Pollmann, F. Real- and Imaginary-Time Evolution with Compressed Quantum Circuits. *PRX Quantum* **2021**, *2*, 010342.
- (54) Jastrow, R. Many-Body Problem with Strong Forces. *Physical Review* **1955**, *98*, 1479–1484.
- (55) Austin, B. M.; Zubarev, D. Y.; Lester, W. A. J. Quantum Monte Carlo and Related Approaches. *Chemical Reviews* **2012**, *112*, 263–288.
- (56) Javadi-Abhari, A.; Treinish, M.; Krsulich, K.; Wood, C. J.; Lishman, J.; Gacon, J.; Martiel, S.; Nation, P. D.; Bishop, L. S.; Cross, A. W.; Johnson, B. R.; Gambetta, J. M. Quantum computing with Qiskit. 2024.
- (57) Byrd, R. H.; Lu, P.; Nocedal, J.; Zhu, C. A Limited Memory Algorithm for Bound Constrained Optimization. *SIAM Journal on Scientific Computing* **1995**, *16*, 1190–1208.
- (58) <https://github.com/MatthewRHermes/mrh>. 2024; <https://github.com/MatthewRHermes/mrh>.
- (59) Sun, Q.; Berkelbach, T. C.; Blunt, N. S.; Booth, G. H.; Guo, S.; Li, Z.; Liu, J.; McClain, J. D.; Sayfutyarova, E. R.; Sharma, S.; Wouters, S.; Chan, G. K.-L. PySCF: the Python-based simulations of chemistry framework. *WIREs Computational Molecular Science* **2018**, *8*, e1340.
- (60) Monino, E.; Boggio-Pasqua, M.; Scemama, A.; Jacquemin, D.; Loos, P.-F. Reference Energies for Cyclobutadiene: Automerization and Excited States. *The Journal of Physical Chemistry A* **2022**, *126*, 4664–4679.

- (61) Dunning, J., Thom H. Gaussian basis sets for use in correlated molecular calculations. I. The atoms boron through neon and hydrogen. *The Journal of Chemical Physics* **1989**, *90*, 1007–1023.
- (62) Kuroiwa, K.; Nakagawa, Y. O. Penalty methods for a variational quantum eigensolver. *Physical Review Research* **2021**, *3*, 013197.
- (63) Huang, H.-Y.; Kueng, R.; Preskill, J. Predicting many properties of a quantum system from very few measurements. *Nature Physics* **2020**, *16*, 1050–1057.
- (64) Zhao, A.; Rubin, N. C.; Miyake, A. Fermionic Partial Tomography via Classical Shadows. *Physical Review Letters* **2021**, *127*, 110504.
- (65) Motta, M.; Ye, E.; McClean, J. R.; Li, Z.; Minnich, A. J.; Babbush, R.; Chan, G. K.-L. Low rank representations for quantum simulation of electronic structure. *npj Quantum Information* **2021**, *7*, 83.
- (66) Berry, D. W.; Gidney, C.; Motta, M.; McClean, J. R.; Babbush, R. Qubitization of Arbitrary Basis Quantum Chemistry Leveraging Sparsity and Low Rank Factorization. *Quantum* **2019**, *3*, 208.
- (67) Huggins, W. J.; McClean, J. R.; Rubin, N. C.; Jiang, Z.; Wiebe, N.; Whaley, K. B.; Babbush, R. Efficient and noise resilient measurements for quantum chemistry on near-term quantum computers. *npj Quantum Information* **2021**, *7*, 23.
- (68) Choi, S.; Loaiza, I.; Izmaylov, A. F. Fluid fermionic fragments for optimizing quantum measurements of electronic Hamiltonians in the variational quantum eigensolver. *Quantum* **2023**, *7*, 889.
- (69) Verteletskyi, V.; Yen, T.-C.; Izmaylov, A. F. Measurement optimization in the variational quantum eigensolver using a minimum clique cover. *The Journal of Chemical Physics* **2020**, *152*, 124114.

- (70) Yen, T.-C.; Verteletskyi, V.; Izmaylov, A. F. Measuring All Compatible Operators in One Series of Single-Qubit Measurements Using Unitary Transformations. *Journal of Chemical Theory and Computation* **2020**, *16*, 2400–2409.
- (71) Bravyi, S. B.; Kitaev, A. Y. Fermionic Quantum Computation. *Annals of Physics* **2002**, *298*, 210–226.
- (72) Seeley, J. T.; Richard, M. J.; Love, P. J. The Bravyi-Kitaev transformation for quantum computation of electronic structure. *The Journal of Chemical Physics* **2012**, *137*, 224109.
- (73) Arrasmith, A.; Cincio, L.; Somma, R. D.; Coles, P. J. Operator Sampling for Shot-frugal Optimization in Variational Algorithms. 2020; <https://arxiv.org/abs/2004.06252>.
- (74) Menickelly, M.; Ha, Y.; Otten, M. Latency considerations for stochastic optimizers in variational quantum algorithms. *Quantum* **2023**, *7*, 949.
- (75) Sung, K. J.; Yao, J.; Harrigan, M. P.; Rubin, N. C.; Jiang, Z.; Lin, L.; Babbush, R.; McClean, J. R. Using models to improve optimizers for variational quantum algorithms. *Quantum Science and Technology* **2020**, *5*, 044008.
- (76) AbuGhanem, M. IBM Quantum Computers: Evolution, Performance, and Future Directions. 2024; <https://arxiv.org/abs/2410.00916>.

TOC Graphic

